

Accretion disc formation around the neutron star in Be/X-ray binaries

Kimitake Hayasaki^{1*} and Atsuo T. Okazaki²

¹*Division of Physics, graduate school of science, Hokkaido University, Kitaku, Sapporo 060-0810, Japan.*

²*Faculty of Engineering, Hokkai-Gakuen University, Toyohira-ku, Sapporo 062-8605, Japan.*

Received; accepted ...

ABSTRACT

We study the accretion on to the neutron star in Be/X-ray binaries, using a 3D SPH code and the data imported from a simulation by Okazaki et al. (2002) for a coplanar system with a short period ($P_{\text{orb}} = 24.3$ d) and a moderate eccentricity ($e = 0.34$), which targeted the Be/X-ray binary 4U 0115+63. For simplicity, we adopt the polytropic equation of state. We find that a time-dependent accretion disc is formed around the neutron star regardless of the simulation parameters. In the long term, the disc evolves via a two-stage process, which consists of the initial developing stage and the later developed stage. The developed disc is nearly Keplerian. In the short term, the disc structure modulates with the orbital phase. The disc shrinks at the periastron passage of the Be star and restores its radius afterwards. The accretion rate on to the neutron star is also phase dependent, but its peak is broader and much lower than that of the mass-transfer rate from the Be disc, unless the polytropic exponent is as large as $5/3$. Our simulations show that the truncated Be disk model for Be/X-ray binaries is consistent with the observed X-ray behaviour of 4U 0115+63.

Key words: accretion, accretion discs – hydrodynamics – methods: numerical – binaries: general – stars: emission-line, Be – X-rays: binaries

1 INTRODUCTION

The Be/X-ray binaries represent the largest subclass of high-mass X-ray binaries. About two-thirds of the identified systems fall into this category. These systems consist of, generally, a neutron star and a Be star with a cool ($\sim 10^4$ K) equatorial disc, which is geometrically thin and nearly Keplerian. The orbit is wide ($16 \text{ d} \lesssim P_{\text{orb}} \lesssim 243 \text{ d}$) and usually eccentric ($e \gtrsim 0.3$) (e.g., Ziolkowski 2002).

Most of the Be/X-ray binaries show only transient activity in the X-ray emission and are termed Be/X-ray transients. Be/X-ray transients show periodical (Type I) outbursts, which are separated by the orbital period and have the lumiosity of $L_X = 10^{36-37} \text{ erg s}^{-1}$, and giant (Type II) outbursts of $L_X \gtrsim 10^{38} \text{ erg s}^{-1}$ with no orbital modulation. The transient nature in the X-ray activity of Be/X-ray binaries is considered to result from the interaction between the accreted material from the circumstellar disc of the Be star and the rotating magnetized neutron star (Stella, White & Rosner 1986). If the accreted material is dense enough to make the magnetospheric radius smaller than the corotation radius, the accretion on to the neutron

star causes a bright X-ray emission (the direct accretion regime). Otherwise, the magnetospheric radius is larger than the corotation radius, and the accretion is prevented by the centrifugal inhibition. The system is then in quiescence (the propeller regime).

During the outbursts, the neutron stars in most Be/X-ray binaries show the spin-ups (e.g., 4U 0115+63, GS 1843-02, EXO 2030+375 and XTE J1946+26) (Bildsten et al. 1997; Finger et al. 1999; Wilson et al. 2002; Wilson et al. 2003), and even some show the quasi-periodic oscillations (QPOs) (e.g., A 0535+26 and EXO 2030+375) (Finger et al. 1996; Wilson et al. 2002). These observational features strongly suggest the presence of the accretion disc during the outbursts.

The accretion disc is also indicated to exist between the outbursts in several systems (e.g., A 0535+26) (Finger et al. 1996; see also Ziolkowski 2002). On the other hand, Clark et al. (1999) searched the optical/infrared contribution from the accretion disc in A 0535+26 during the X-ray quiescent phase, and found no signature of the accretion disc in propeller regime. Obviously, more work is needed to determine whether the accretion disc also exists in the quiescent state.

* E-mail: kimi@astro1.sci.hokudai.ac.jp

Recently, Okazaki et al. (2002) studied the interac-

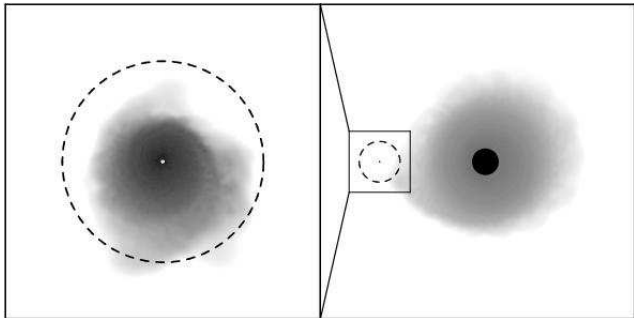


Figure 1. Illustrative diagram of a Be/X-ray binary. At the periastron passage, the gas in an outer part of the Be-star disc is transferred to the neutron star and forms an accretion disc. The right panel is taken from a simulation by Okazaki et al. (2002), while the left panel is from one of our simulations.

tion between the Be-star disc and the neutron star, using a three-dimensional (3D) smoothed particle hydrodynamics (SPH) code (Benz 1990; Bate, Bonnell & Price 1995). They also qualitatively discussed the relation between the X-ray luminosity and the accretion rate using the simulated mass-capture rate by the neutron star. In their simulations, however, the neutron star was modelled by a sink particle (Bate et al. 1995) with the size of the Roche lobe. Hence, no information was available how the captured material accretes on to the neutron star. Moreover, no direct comparison with the observed X-ray data was possible.

In this paper, we study the accretion on to the neutron star in Be/X-ray binaries, using a 3D SPH code. The simulation should ideally take account of all the processes at work in a Be/X-ray binary, such as the disc evolution around the Be star, the mass transfer from the Be-star disc to the neutron star, and the accretion on to the neutron star. Such a simulation, however, would require very intense computations.

Therefore, we confine ourselves to simulate only the accretion flow around the neutron star, with an outer boundary condition constructed by the data of the particles captured by the neutron star from a high-resolution simulation by Okazaki et al. (2002). This situation is illustrated in Fig. 1, where the right panel taken from their simulation shows the mass transfer from the Be-star disc to the neutron star at periastron, while the left panel shows the accretion disc formed around the neutron star in one of our simulations.

2 NUMERICAL MODEL

2.1 SPH code

Simulations presented here were performed with a 3D SPH code. The SPH code is basically the same as that used by Okazaki et al. (2002), which is based on a version originally developed by Benz (Benz 1990; Benz et al. 1990). The smoothing length is variable in time and space. The SPH equation with the standard cubic-spline kernel are integrated using a second-order Runge-Kutta-Fehlberg integrator with individual time steps for each particle (Bate et al. 1995), which results in an enormous computational saving when a large range of dynamical time-scales are involved.

In our code, the accretion flow on to the neutron star is modelled by an ensemble of gas particles, each of which has a negligible mass chosen to be $10^{-15}M_{\odot}$ with a variable smoothing length. For simplicity, the gas particles are assumed to be polytropic. On the other hand, the Be star and the neutron star are modelled by two sink particles (Bate et al. 1995) with corresponding masses. The gas particles which fall within a specified accretion radius are accreted by the sink particles. We assume that the neutron star has the fixed accretion radius of $3.0 - 5.0 \times 10^{-3}a$, a being the semi-major axis of the binary. For the Be star, we adopt a variable accretion radius of $0.8r_L$, where r_L is the Roche-lobe radius for a circular binary. This is because our interest is only in the flow around the neutron star. An approximate formula for r_L is given by

$$r_L \simeq 0.462 \left(\frac{1}{1+q} \right)^{1/3} D, \quad (1)$$

(see, for example, Warner 1995; Frank, King & Raine 2002) with the mass ratio $q = M_X/M_*$, where M_X and M_* are the masses of the neutron star and the Be star, respectively, and D is the distance between the stars.

In disc simulations using a three dimensional SPH code with the standard cubic spline kernel, one has an approximate relation between the Shakura-Sunyaev viscosity parameter α_{SS} and the linear SPH artificial viscosity parameter α_{SPH} as

$$\alpha_{SS} = \frac{1}{10} \alpha_{SPH} \frac{h}{H}, \quad (2)$$

where h is the SPH smoothing length and H is the scale-height of the disc (Okazaki et al. 2002). In a simulation we report in this paper, we adopt $\alpha_{SPH} = 1$ and $\beta_{SPH} = 2$, in which case α_{SS} is variable in time and space. In the other simulations, however, we adopt a constant value of α_{SS} in order to roughly model the α disc. In these simulations, $\alpha_{SPH} = 10\alpha_{SS}H/h$ was variable in time and space and $\beta_{SPH} = 0$.

In our simulations, we adopt a polytropic equation of state specified by the exponent Γ , in which the effects of an energy dissipation resulting from viscosity and a radiative cooling are approximately boxed.

2.2 Boundary condition

Our binary configuration is the same as that of Okazaki et al. (2002). We set the binary orbit on the x - y plane with the semi-major axis along the x -axis. Initially, the neutron star is at the periastron. It orbits about the Be star with the orbital period $P_{orb} = 24.3$ d and the eccentricity $e = 0.34$. The Be disc is coplaner with the binary orbital plane. As the Be star, we take a B0V star with $M_* = 18M_{\odot}$, $R_* = 8R_{\odot}$ and $T_{eff} = 26000$ K, where R_* and T_{eff} are the stellar radius and effective temperature, respectively. For the neutron star, we take $M_X = 1.4M_{\odot}$ and $R_X = 10^6$ cm. These parameters are adopted to target 4U 0115+63, which has shown only Type II X-ray outbursts followed by a short series of Type I X-ray outbursts (Negueruela et al. 2001).

As mentioned earlier, we concentrate only on the simulations of the accretion flow on to the neutron star. This is done by constructing an outer boundary condition from

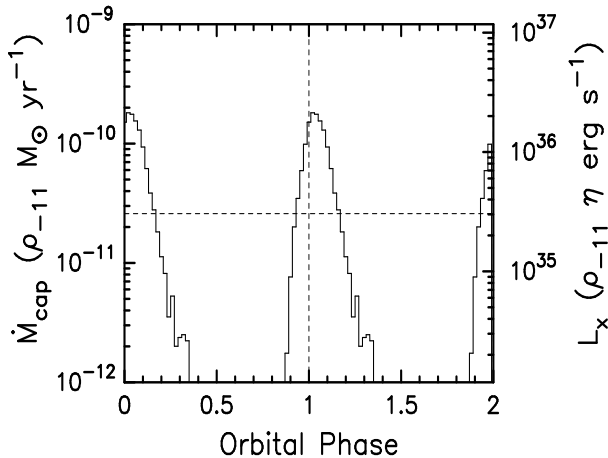


Figure 2. Orbital-phase dependence of the mass-capture rate by the neutron star, taken from a high-resolution simulation by Okazaki et al. (2002). The data is folded on the orbital period over $32 \leq t \leq 47$. The mass-capture rate is measured in units of $\rho_{-11} M_{\odot} \text{ yr}^{-1}$, where ρ_{-11} is highest local density in the Be-star disc normalized by $10^{-11} \text{ g cm}^{-3}$, a typical value for Be stars. The right axis shows the X-ray luminosity corresponding to the mass-capture rate with the X-ray emission efficiency $\eta = 1$, where η is defined by $L_X = \eta M_X \dot{M}_{\text{cap}} / R_X$.

the data of particles captured by the neutron star in a high-resolution simulation by Okazaki et al. (2002), which was run for $0 \leq t \leq 47$ and finally had ~ 140000 particles with $\alpha_{\text{SS}} = 0.1$. We first fold the data on the orbital period over $32 \leq t \leq 47$ to reduce the fluctuation noise. The phase dependence of the mass-capture rate by the neutron star obtained by this procedure is shown in Fig. 2. Note that there is a strong phase-dependence in the mass-transfer rate. The peak comes slightly after the periastron passage and decreases by two orders of magnitude by apastron passage. We then fit the spatial and velocity distribution of the captured particles in each phase bin with separate Gaussian functions. This is for running simulations with an arbitrary mass-transfer rate from the Be disc. We finally model the mass-transfer process from the Be disc to the neutron star by injecting gas particles at a given phase-dependent rate shown in Fig. 2 with the spatial and velocity distributions specified by these Gaussian functions. The injected particles are assumed to have the initial temperature of $T_{\text{eff}}/2$.

2.3 Possibility of an accretion disc formation

Before describing the results of our simulations, we discuss below the possibility of the formation of an accretion disc around the neutron star.

We first consider the radius R_{circ} at which the material transferred from the Be disc is circularized via the interaction with the previously transferred gas. We assume the circularization radius R_{circ} to be approximately given by $R_{\text{circ}} = J^2 / GM_X$, where J is the initial specific angular momentum of the transferred material.

In the upper panel of Fig. 3, we show the dependence of R_{circ} on the orbital phase, based on the data taken from a simulation by Okazaki et al. (2002). It is noted that there is a strong phase-dependence of R_{circ} . It has a minimum of $\sim 10^{-4} a$ slightly before periastron and then rapidly increases

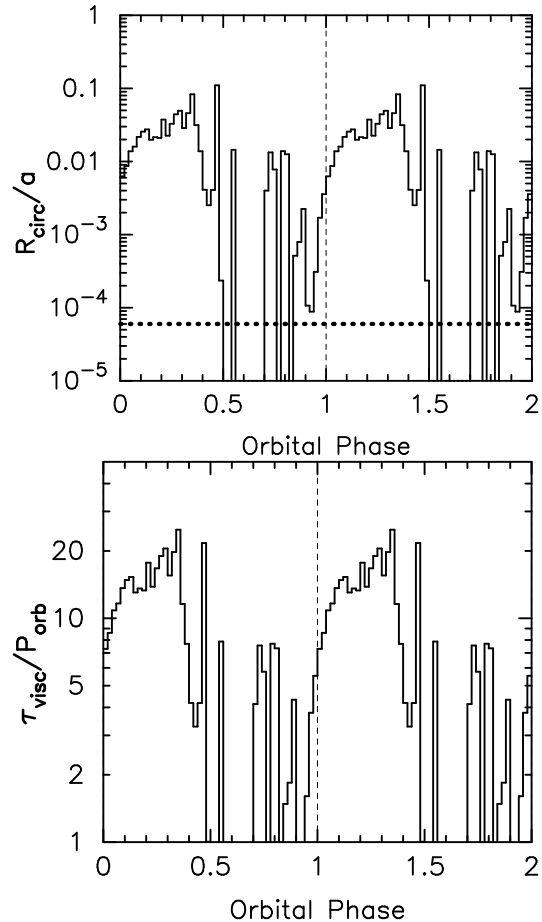


Figure 3. Orbital-phase dependence of the circularization radius (the upper panel) and the ratio of the viscous time-scale to the orbital period (the lower panel) for the gas transferred from the Be disc in 4U 0115+63, based on the data imported from a simulation by Okazaki et al. (2002). The horizontal dotted line in the upper panel denotes the corotation radius $R_{\Omega} = 6.0 \times 10^{-5} a$.

with phase. For comparison, we also show the corotation radius, R_{Ω} , for 4U 0115+63 by the dotted line. Here, R_{Ω} is given by

$$R_{\Omega} = \left(\frac{GM_X P_{\text{spin}}^2}{4\pi^2} \right)^{1/3} = 1.5 \times 10^8 P_{\text{spin}}^{2/3} \left(\frac{M_X}{M_{\odot}} \right)^{1/3} \text{ cm}, \quad (3)$$

where $P_{\text{spin}} = 3.61$ s is the spin period of the neutron star in 4U 0115+63. Note that $R_{\text{circ}} \gg R_{\Omega}$ for most of the orbital phase. Therefore, we expect that an accretion disc is formed around the neutron star in 4U 0115+63.

Next, we discuss whether the accretion disc formed around the neutron star is persistent or transient. This is done by comparing the viscous accretion time-scale with the orbital period. For simplicity, we assume the accretion disc to be geometrically thin and isothermal with the Shakura-Sunyaev viscosity parameter α_{SS} and evaluate the accretion time-scale at $r = R_{\text{circ}}$. The ratio of these two time-scales for 4U 0115+63 is then given by

$$\begin{aligned} \frac{\tau_{\text{vis}}}{P_{\text{orb}}} &\sim \frac{1}{2\pi\alpha_{\text{SS}}c_s^2} \left(\frac{R_{\text{circ}}}{a} \right)^{1/2} \frac{GM_X}{a} \left(1 + \frac{1}{q} \right)^{1/2}, \\ &\sim 1.2 \times 10^2 \left(\frac{\alpha_{\text{SS}}}{0.1} \right)^{-1} \left[\frac{R_{\text{circ}}}{a} \right]^{1/2} \left(\frac{T_d}{10^4 \text{ K}} \right)^{-1}, \end{aligned} \quad (4)$$

Table 1. Summary of models of our simulations. The initial number of particles is 301 and the mean mass injection rate is $2.5 \times 10^{-11} \rho_{-11} M_{\odot} \text{yr}^{-1}$ in all simulations. The first column represents the model. The second column is the polytropic exponent Γ and the third column is the number of SPH particles at the end of the run, which is given in units of P_{orb} in the fourth column. The viscosity parameters adopted are given in the fifth column and the sixth column is the inner radius of the simulation region. The seventh column is the number of injected particles for one orbital period. The last two columns are the number of accreted particles for the last one orbital period and the corresponding mean accretion rate, respectively.

Model	Polytropic exponent Γ	N_{SPH} (final)	Run time (P_{orb})	Viscosity parameters	Inner boundary r_{in}/a	N_{inj}	N_{acc}	\dot{M}_{acc} ($\rho_{-11} M_{\odot} \text{yr}^{-1}$)
1	1.2	45687	8	$\alpha_{\text{SS}} = 0.1$	3.0×10^{-3}	8657	2990	8.3×10^{-12}
2	1.2	35821	8	$\alpha_{\text{SS}} = 0.1$	5.0×10^{-3}	8717	4054	1.1×10^{-11}
3	1 (isothermal)	39295	8	$\alpha_{\text{SS}} = 0.1$	5.0×10^{-3}	8844	2676	7.4×10^{-12}
4	5/3 (adiabatic)	20118	8	$\alpha_{\text{SS}} = 0.1$	5.0×10^{-3}	8594	6851	1.9×10^{-11}
5	1.2	47730	8	$\alpha_{\text{SPH}} = 1, \beta_{\text{SPH}} = 2$	5.0×10^{-3}	8705	2671	7.5×10^{-12}
6	1.2	17488	1	$\alpha_{\text{SS}} = 0.1$	5.0×10^{-3}	34778	16829	1.2×10^{-11}

where c_s is the sound speed and T_d is the disc temperature. The orbital-phase dependence of $\tau_{\text{vis}}/P_{\text{orb}}$ is shown in the lower panel of Fig. 3. It is immediately observed that the viscous accretion time-scale is much longer than the orbital period for most of the orbital phase. Therefore, once formed, the accretion disc around the neutron star in 4U 0115+63 will survive over the whole orbital phase. Note that this result depends little on the orbital period, since equation (4) is insensitive to P_{orb} .

3 ACCRETION FLOW AROUND THE NEUTRON STAR

Based on the procedure described in the previous section, we have performed several simulations with different parameters. Details of the models are given in Table 1. The polytropic exponent considered are $\Gamma = 1$ (model 3), 1.2 (models 1, 2, 5 and 6) and 5/3 (model 4). We have taken the inner radius of the simulation region, r_{in} , to be $5.0 \times 10^{-3} a$ in all simulations but model 1 with a smaller inner radius of $r_{\text{in}} = 3.0 \times 10^{-3} a$, which was run to study the effect of the inner radius on the simulation results. In models 1-4 and 6, we have assumed $\alpha_{\text{SS}} = 0.1$, where α_{SPH} varies in time and space and $\beta_{\text{SPH}} = 0$. For comparison purpose, we have also run model 5 with $\alpha_{\text{SPH}} = 1$ and $\beta_{\text{SPH}} = 2$, where α_{SS} varies in time and space. Model 6 was run solely for clearly illustrating the initial build-up phase of an accretion disc. For this purpose, we have taken the injection rate of the SPH particles in model 6 four times as high as in other models and run only for one orbital period.

Analysing multi-wavelength long term monitoring observations of 4U 0115+63, Negueruela et al. (2001) found that the Be star undergoes quasi-cyclic ($\sim 3 - 5$ yr) activity, losing and reforming its circumstellar disc. Then, the mass transfer to the neutron star should vary, depending on the state of the Be disc. By the time the Be disc is fully developed and becomes capable of supplying mass to the neutron star, even a large accretion disc would be exhausted. Therefore, to investigate the evolution of an accretion flow around the neutron star after the Be disc is fully developed, we performed 3D SPH simulations based on the numerical models described above, where there is initially no gas particle around the neutron star. Since all models have shown similar structure and evolution of the accretion flow, we will mainly show the results from model 1 with $\Gamma = 1.2$ and $r_{\text{in}} = 3 \times 10^{-3} a$.

3.1 Initial phase of the disc formation

We consider the initial phase of accretion flow around the neutron star. As discussed in Section 2.3, it is expected that the material transferred from the Be disc near the periastron does not directly fall on to the neutron star and forms a disc-like structure with a size corresponding to its specific angular momentum.

For illustration purpose, we give in Fig. 4 the snapshots of the initial accretion flow around the neutron star from model 6, which covers $t = 0 - 1$. At $t = 0$, the Be star is at periastron. Each panel shows the surface density in the range of four orders of magnitude in the logarithmic scale. We note that the accreting matter first forms an elliptical ring around the neutron star, which is then relaxed to an elliptical disc via the viscous diffusion. Because of the viscous time-scale longer than the orbital period, the orbits of the accreting particles are not circularized and the flow is highly eccentric during the initial phase of accretion. Comparing the number of particles, N_{SPH} , with the number of particles inside the effective Roche radius of the neutron star, N_{Roche} , we also note that most of the material transferred from the Be disc stays inside the effective Roche radius of the neutron star. It should be noted that these dynamical features are common to all models studied in this paper.

Fig. 5 shows the orbital-phase dependence of the radial structure of the accretion flow around the neutron star at the same times as in Fig. 4. In each panel, the solid line, the dashed line and the dash-dotted line denote the surface density Σ , the azimuthal velocity v_{ϕ} normalized by the Keplerian velocity at the inner boundary and the radial Mach number v_r/c_s , respectively. In the figure, the density is integrated vertically and averaged azimuthally, while the velocity components are averaged vertically and azimuthally. From Fig. 5 we note that while the azimuthal velocity distribution gradually approaches the Keplerian one, the behaviour of the radial velocity is very complex, reflecting the dynamical process of the disc formation shown in Fig. 4.

The surface density distribution also shows the initial evolution of the accretion flow described above. In the panel at $t = 0.12$, there appears a hump at $r \sim 0.08a$ caused by the infall of injected particles. Outside the hump the density decreases rapidly, making a ring-like structure with a sharp outer edge. This rapid decrease in the density is due to the ram pressure of the infalling particles. As the hump moves inward, the density gradient outside the hump becomes less

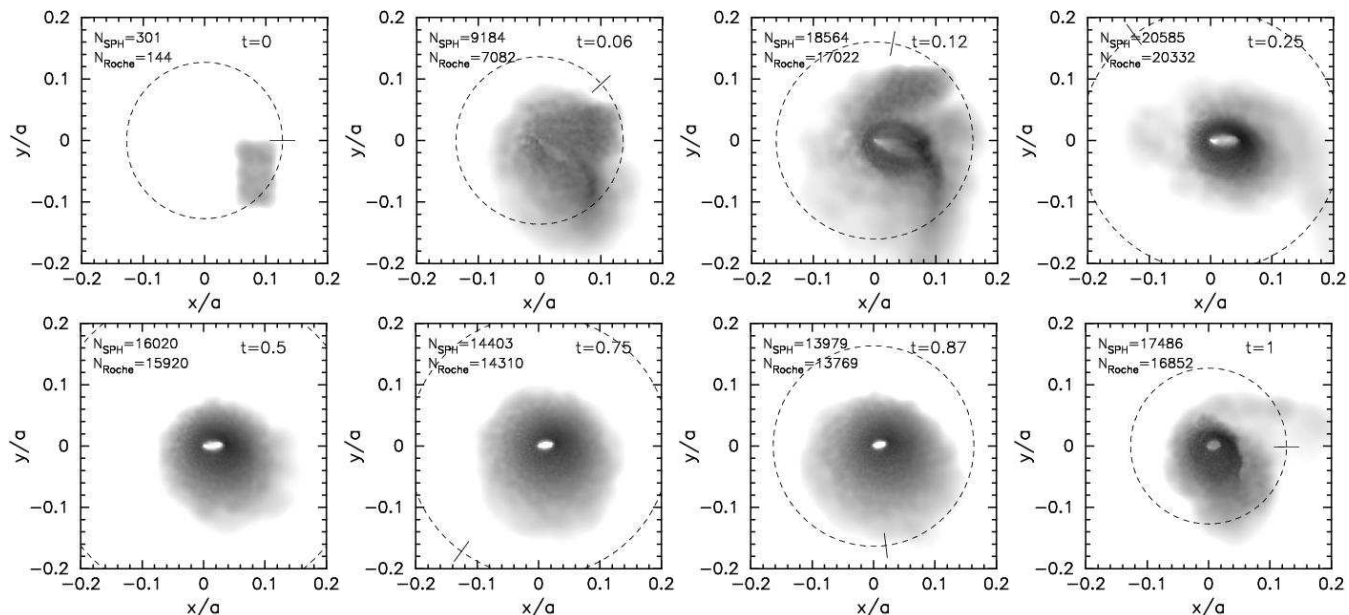


Figure 4. A sequence of snapshots showing the initial phase ($t = 0 - 1$) of the disc formation around the neutron star in model 6 with $\Gamma = 1.2$ and $r_{\text{in}} = 5 \times 10^{-3} a$. The origin is set on the neutron star. Each panel shows the surface density in a range of four orders of magnitude in the logarithmic scale. The dashed circle denotes the effective Roche lobe of the neutron star. The short line-segment indicates the direction of the Be star. The unit of time is the orbital period P_{orb} . Annotated at the top-left corner of each panel are the number of SPH particles, N_{SPH} , and the number of particles inside the effective Roche lobe of the neutron star, N_{Roche} .

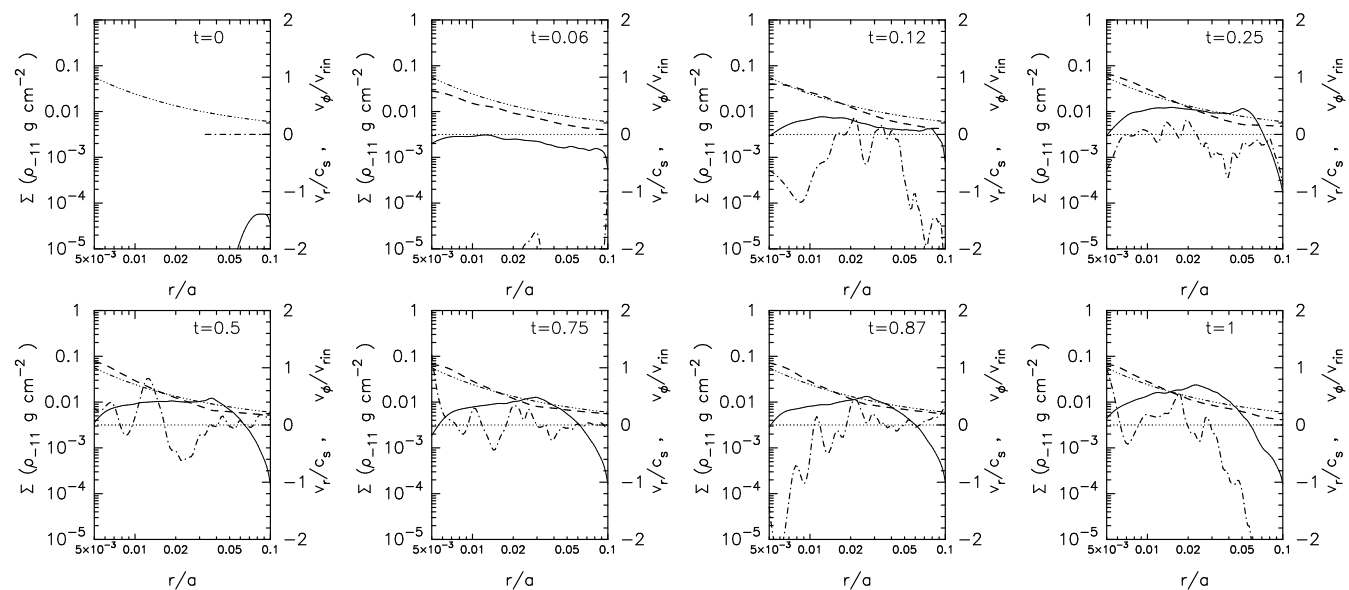


Figure 5. Orbital-phase dependence of the radial structure of the accretion flow shown in Fig. 4. In each panel, the solid line, the dashed line and the dash-dotted line denote the surface density Σ in units of $\rho_{-11} \text{ g cm}^{-2}$, the azimuthal velocity v_ϕ normalized by the Keplerian velocity at the inner boundary and the radial Mach number v_r/c_s , respectively. For comparison, the Keplerian velocity distribution is shown by the dash-three-dotted line. The density is integrated vertically and averaged azimuthally, while the velocity components are averaged vertically and azimuthally.

step. By the next periastron passage ($t = 1$), a disc-like structure is formed, the inner radius of which is at $r \simeq 0.02a$.

In our simulations, the presence of the inner simulation boundary causes an artificial decrease in the density near the boundary, because the gas particles which pass through the boundary are removed from the simulation. As a result, the density distribution has a break near the inner boundary,

as seen in Fig. 5. We have found that our simulations are reliable for $\gtrsim 2r_{\text{in}}$.

3.2 Structure of a developed disc

Many Be/X-ray binaries with known orbital parameters have orbital eccentricities in the range of 0.3 to 0.9. In

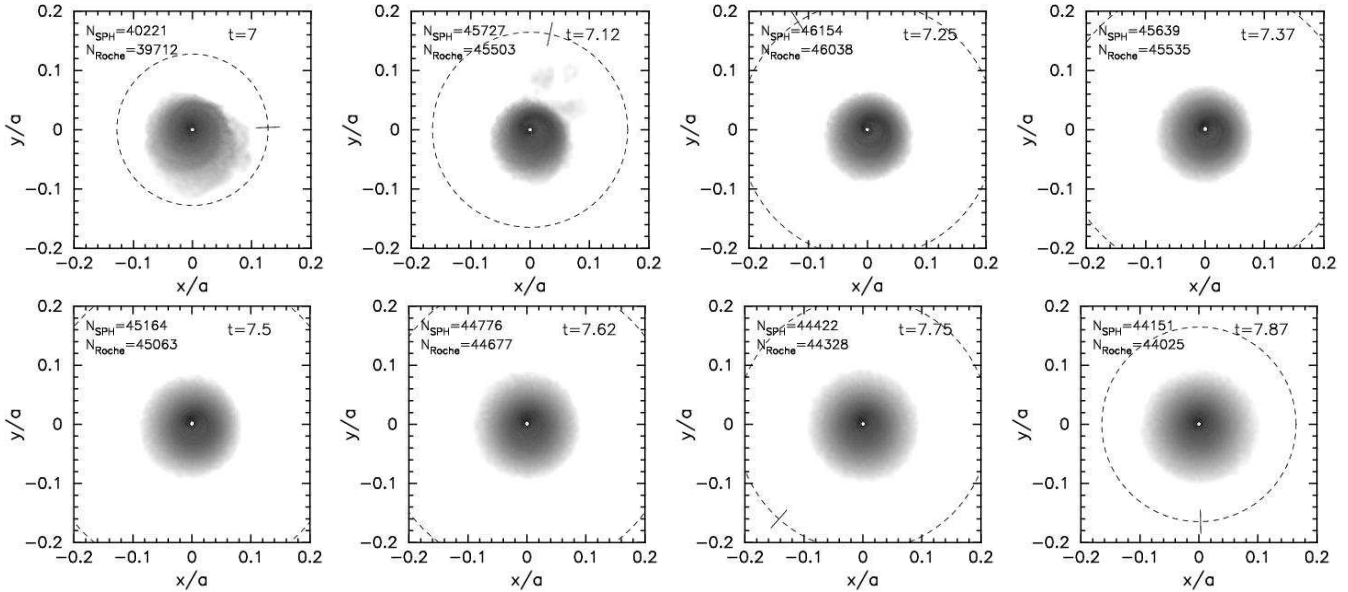


Figure 6. A sequence of snapshots of a developed accretion disc in model 1, which cover one orbital period ($t = 7 - 8$). The format of the figure is the same as that of Fig. 4, except that the surface density is shown in a range of three orders of magnitude in the logarithmic scale.

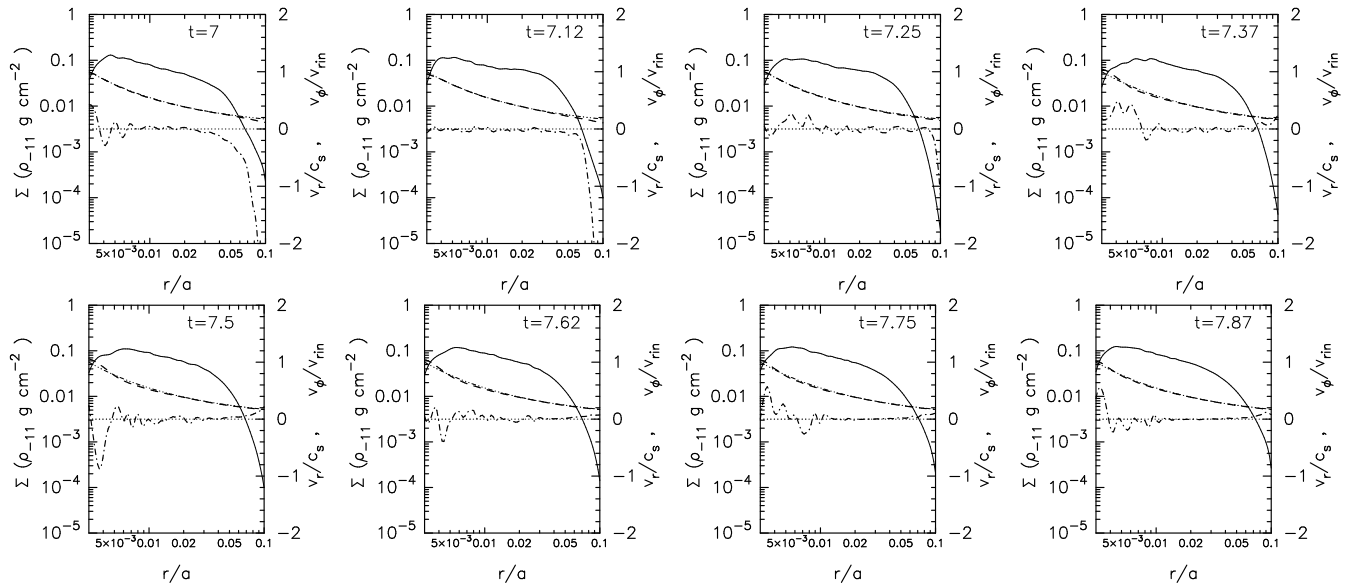


Figure 7. Orbital-phase dependence of the radial structure of the developed accretion disc shown in Fig. 6. The format of the figure is the same as that of Fig. 5.

such systems, the mass-transfer rate from the Be disc is expected to have the strong phase dependence (Okazaki et al. 2002). Accordingly, the structure of an accretion disc formed around the neutron star in these systems is also likely to be strongly phase dependent. In this section, we first discuss the phase-dependent structure of a developed accretion disc in model 1 and then compare that with those in other models.

3.2.1 Model 1

Fig. 6 gives a sequence of snapshots of the accretion flow around the neutron star covering one orbital period for $7 \leq$

$t < 8$. The format of the figure is the same as that of Fig. 4, except that the surface density is shown in the range of three orders of magnitude. We note from the figure that the disc shrinks at periastron passage by a negative torque exerted by the Be star and restores its radius afterwards by the viscous diffusion. We also note that the disc is significantly eccentric even after it is fully developed, although the eccentricity is much smaller than that in the initial phase of the disc formation.

Fig. 7 shows the radial disc structure at the orbital phases corresponding to Fig. 6. The format of the figure is the same as that of Fig. 5. It is noted from Fig. 7 that the disc is nearly Keplerian at any phase and the accretion flow

is highly subsonic except in the outermost part for a short period of time when the material transferred from the Be disc falls towards the neutron star. We call this state of the accretion disc developed. We have found that these features of a developed disc hold for $t \gtrsim 5$ in model 1. As in the initial phase of the disc formation, the ram pressure by the supersonic infall of matter transferred from the Be disc around periastron enhances the density in the outermost part of the accretion disc, making the disc outer edge sharp (see panels for $7.12 \leq t \leq 7.37$ in Figs. 6 and 7). Afterwards, the disc gradually expands until the next periastron passage of the Be star.

3.2.2 Models 2-5

In this section, we describe the effects of the simulation parameters in Table 1 on the structure of the accretion flow around the neutron star.

We ran model 2 to study the effect of the inner boundary on the disc structure. Fig. 8 shows the snapshots and the radial structures of the accretion flow around the neutron star at $t = 7$ (periastron) and $t = 7.5$ (apastron) for model 2, which has the same simulation parameters as model 1, except for a larger inner boundary of $r_{\text{in}} = 5 \times 10^{-3}$. Comparing Fig. 8 with the panels at the corresponding times in Figs. 6 and 7 for model 1, we note that the presence of the inner boundary artificially reduces the density in a narrow region ($r \lesssim 2r_{\text{in}}$) near the boundary, but outside of it, the disc structure is similar for both models.

In order to study the dependence of the disc structure on the polytropic exponent, we also ran models 3 ($\Gamma = 1$; isothermal case) and 4 ($\Gamma = 5/3$; adiabatic case), for which the polytropic exponent of 1.2 for models 1, 2 and 6 is in between. Fig. 9 shows the snapshots and the radial structures of the accretion disc for model 3 (isothermal case) at the same times as in Fig. 8. From the figure, we note that the distributions of the surface density and both of the azimuthal and radial velocity components are similar to those in the initial phase of the disc formation for $\Gamma = 1.2$ (see Figs. 4 and 5). Consequently, in model 3 the accretion disc is still developing at $t \sim 7$. This is because the viscous time-scale of the isothermal disc, particularly in an inner region, is longer than those in the other models (see also Fig. 3).

Fig. 10 shows the disc structure for model 4 (adiabatic case). We note that the disc is nearly Keplerian at both orbital phases and that the surface density is lower and the disc is bigger than those for model 2 with $\Gamma = 1.2$. This is due to a higher viscous stress in model 4, resulting from a higher pressure. As expected, in model 4, the accretion rate is much higher than the models with lower polytropic exponents, which we will see in a later section.

We also studied a model with the standard, artificial viscosity parameters. Model 5 has the same simulation parameters as those in model 2, except that it has constant artificial viscosity parameters $\alpha_{\text{SPH}} = 1$ and $\beta_{\text{SPH}} = 2$, for which α_{SS} varies in time and space. Fig. 11 shows the disc structure for model 5. It is immediately noted that the inner boundary affects the disc structure much more widely in this model. This is mainly because the inner disc region is not resolved vertically for this number of SPH particles. Since the ratio of the smoothing length to the disc scale-height h/H in the inner region is much higher than unity, the shear vis-

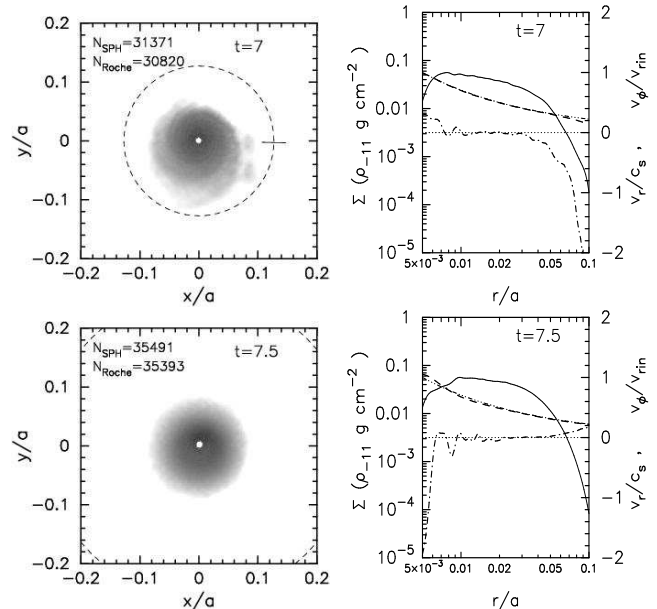


Figure 8. Orbital-phase dependence of the accretion disc structure in model 2. The top panels show the snapshot (left) and the radial structure (right) at the periastron, while the bottom panels show those at the apastron. In the snapshots, the surface density is shown in a range of three orders of magnitude in the logarithmic scale.

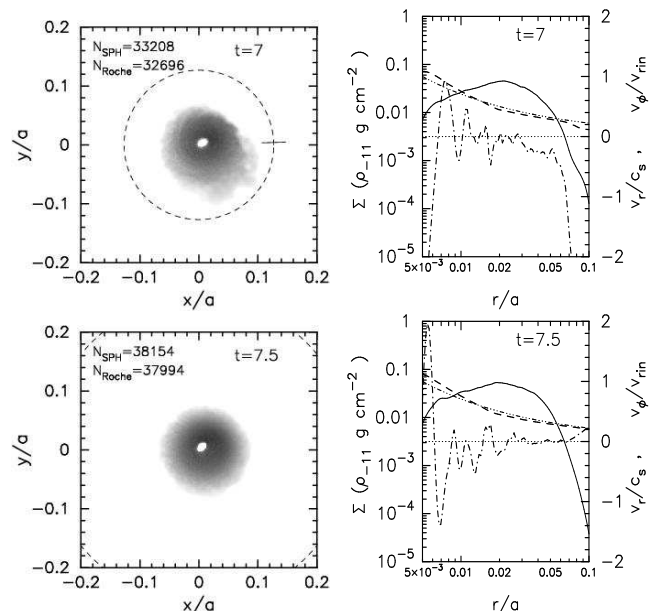


Figure 9. Same as Fig. 8, but for model 3.

cosity parameter α_{SS} in this model is much higher in the inner region than that in the other models.

Except for the above-mentioned dependence of the disc structure on the simulation parameters, the accretion discs in our models share the common features: They are nearly Keplerian after developed and their structures modulate with the orbital phase. They are also significantly eccentric. We will analyse the non-axisymmetry of the accretion discs in Be/X-ray binaries in a subsequent paper.

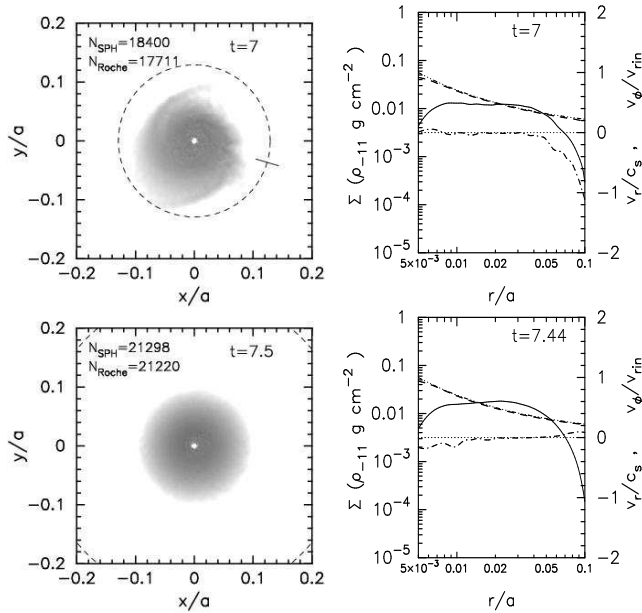


Figure 10. Same as Fig. 8, but for model 4.

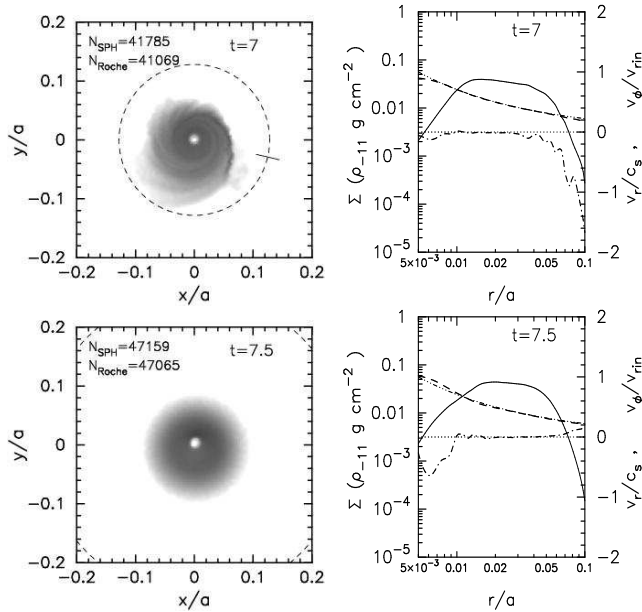


Figure 11. Same as Fig. 8, but for model 5.

3.2.3 Size of the accretion disc in Be/X-ray binaries

Artymowicz & Lubow (1994) investigated the tidal/resonant truncation of circumstellar and circumbinary discs in eccentric binaries and found that a gap is always opened between the disc and the binary orbit. Following their formulation, Negueruela & Okazaki (2001) and Okazaki & Negueruela (2001) have shown that the Be disc is truncated via the resonant interaction with the neutron star, as long as $\alpha_{SS} \ll 1$, which has recently been confirmed by numerical simulations by Okazaki et al. (2002).

It is interesting to study whether the resonant torque by the Be star also truncates the accretion disc around the neutron star. In order to have a measure of the accretion

disc radius at which the disc density has a major break, we have applied a non-linear least squares fitting method to the radial distribution of the azimuthally-averaged surface density Σ , adopting the following simple fitting function,

$$\Sigma \propto \frac{(r/r_d)^{-p}}{1 + (r/r_d)^q}, \quad (5)$$

where p and q are constants and r_d is the radius of accretion disc. This method is the same as that adopted by Okazaki et al. (2002).

Fig. 12 shows the orbital-phase dependence of the accretion disc radius in model 1. To reduce the fluctuation noise, we folded the data on the orbital period over $5 \leq t \leq 8$. It is noted that the disc radius varies between $0.04a$ and $0.05a$. The disc shrinks at periastron due to the resonant torque and gradually restores its radius towards apastron. The rapid increase of the disc radius before periastron is due to the infall of matter from the Be star.

Next, we examine whether the disc radius is determined by the resonant truncation as is the case in the Be disc in Be/X-ray binaries. Fig. 8 of Artymowicz & Lubow (1994) gives the truncation radius as a function of the orbital eccentricity e and the disc Reynolds number Re for systems with the mass ratio of 0.1, which is similar to that of Be/X-ray binaries. Since the accretion disc in our model is geometrically thin and nearly Keplerian, the Reynolds number Re is given by $Re = (1/\alpha_{SS})(r/H)^2 \sim (1/\alpha_{SS})(v_{Kep}/c_s)^2$, where H is the scale-height of the disc and v_{Kep} is the Keplerian velocity. In model 1, $Re \sim 10^{3-3.5}$ for $0.01a \lesssim r \lesssim 0.1a$. From Fig. 8 of Artymowicz & Lubow (1994), with $e = 0.34$ and $Re \sim 10^{3-3.5}$, we have the truncation radius of $\sim 0.14a$, which corresponds to the 6:1 resonance radius. Note that this radius is much larger than the disc radius shown in Fig. 12. Thus, we rule out that the accretion disc is resonantly truncated as is the Be counterpart.

It is suggestive that the disc radius is about the same as the circularization radius R_{circ} of the matter transferred from the Be disc after the periastron passage (see Fig. 3). Since the viscous time-scale at the circularization radius is much longer than the orbital period, the matter once circularized does not change its radius very much over one orbital period. Therefore, we conclude that the size of the accretion disc in Be/X-ray binaries is determined by the specific angular momentum of the matter transferred from the Be disc.

3.3 Disc evolution

As mentioned in Section 1, most of the Be/X-ray binaries show transient X-ray activities, of which nature is considered to result from the interactions between the accreted material and the rotating magnetized neutron star (Stella et al. 1986). In this section, we first describe the growth of the accretion disc in mass and radius. We then examine the evolution of the mass-accretion rate obtained by our simulations, from which we finally discuss the X-ray activity expected in Be/X-ray binaries.

3.3.1 Growth of the disc

Fig. 13(a) shows the evolution of the disk mass in model 1 over the period of $0 \leq t \leq 8$. In the long term, the disc

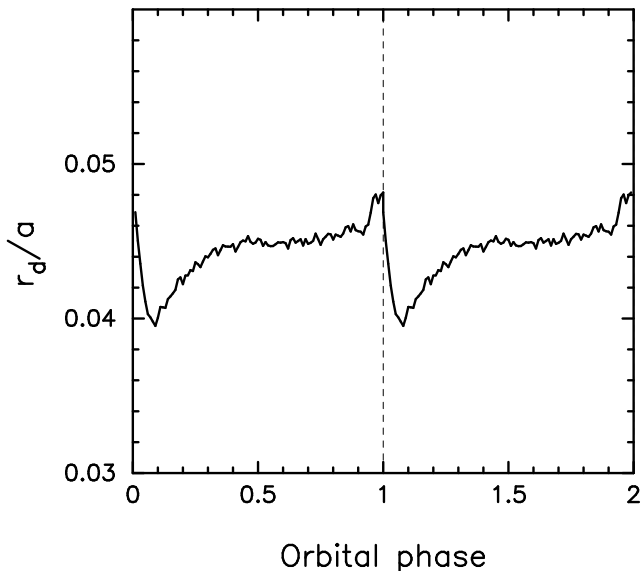


Figure 12. Orbital-phase dependence of the accretion disc radius r_d . To reduce the fluctuation noise, the data was folded on the orbital period for $5 \leq t \leq 8$.

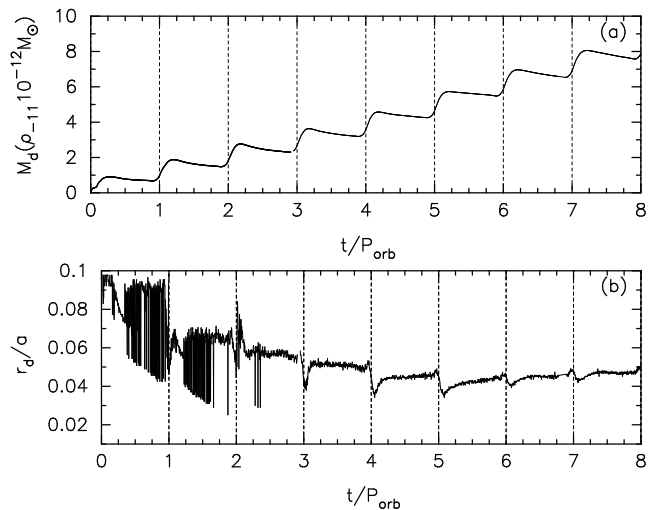


Figure 13. Evolution of (a) the disc mass M_d and (b) the disc size r_d normalized by the semi-major axis for $0 \leq t \leq 8$. In panel (a), the disc mass is measured in units of $\rho_{-11} 10^{-12} M_\odot$.

mass increases with time, because the the gas transferred from the Be star accumulates in the accretion disc because of the viscous time-scale longer than the orbital period. On the other hand, in the short term, it modulates with the orbital phase. The disk mass starts increasing, when the mass-supply from the Be disc begins slightly before every periastron passage. It shows a rapid increase for a short while, followed by a gradual decrease by accretion with no mass-supply from the Be disc, which lasts until the next periastron passage.

In Fig. 13(b), we show the evolution of the disc radius over $0 \leq t \leq 8$. One may expect that the disc radius gradually increases with the disc mass. From the figure, however, we note that this is the case only for $t \gtrsim 5$. In fact, for $t \lesssim 5$, the disc radius decreases as the disc grows. This counter-

intuitive decrease in radius is related to the change in the disc eccentricity. In the early stage of disc formation, the disc/ring is highly eccentric (see Fig. 4), for which the radius r_d calculated by equation (5) is larger than that for a circular disc with the same disc mass. Since the disc eccentricity decreases with time, so does the disk radius. In model 1, the effect of the disc circularization is balanced with that of the disc growth at $t \sim 5$. After this epoch, the disc radius increases with the disc mass. Thus, the evolution of the accretion flow around the neutron star in Be/X-ray binaries involves a two-stage process, which consists of the initial developing stage and the later developed stage.

3.3.2 Phase-dependent accretion

Fig. 14(a) shows the evolution of the mass-accretion rate and the corresponding X-ray luminosity in model 1 for $0 \leq t \leq 8$. The thick and thin lines denote the mass-accretion rate in models 1 and 2, respectively. Note that the mass-accretion rate in our simulations generally has double peaks per orbit. The first peak, which occurs at the periastron, is due to the contraction of the disc by the resonant torque of the Be star, except that the peaks at periastron during the initial phase of disc formation are mainly due to the direct accretion of gas with low specific angular momentum. The second peak, which lags behind the peak in the mass-transfer rate from the Be disc shown in Fig. 2, results from the viscous accretion of matter transferred from the Be disc. The first peak could be artificial since it is related to the presence of the inner simulation boundary.

The orbital modulation in the mass-accretion rate is significantly different between the developing disc and the developed disc. The first peak becomes weak as the disc develops. After the disc is fully developed, the second peak is higher than the first peak.

Fig. 14(a) also shows that, once developed, the accretion disc in 4U 0115+63 shows the peak X-ray luminosity of $L_X \lesssim 2 \cdot 10^{35} \text{ erg s}^{-1}$. This level of X-ray emission enters the transition regime (see Campana et al. 2001) and is consistent with the observed X-ray luminosity in the quiescent state.

For comparison purpose, we present in Fig. 15 the evolution of the mass-accretion rate and the corresponding X-ray luminosity in models 2-4 for $0 \leq t \leq 8$. The thick and thin solid lines and the thin dotted line are for models 2, 3 and 4, respectively. We see from the figure that the accretion rate increases with increasing polytropic exponent. In models 2 ($\Gamma = 1.2$) and 3 ($\Gamma = 1$), the accretion rate profile has the double peaks as described above. The long-term change in the peak profiles is also similar to that in model 1. We note that the disc in model 2 entered the stage of the developed disc at $t \sim 6$. On the other hand, the disc in model 3 is at the developing stage even at $t = 8$, which is consistent with the disc structure shown in Fig. 9.

In contrast to the models with low Γ , the accretion rate in model 4 has a single and periodic peak per orbit, even after the disc is developed. With $\Gamma = 5/3$, the pressure in the disc in model 4 is much higher than that in the other models. This means that much larger viscous torque exerts on the disc in model 4 than in the other models, because the viscous stress in the α -viscosity prescription is proportional to the pressure. As a result, the viscous torque dominates

the resonant torque in model 4 even at periastron. This is why there is no peak at periastron and the accretion rate shows the regular orbital modulation with the amplitude much higher than in the other models.

It is important to note that the disc evolution and its orbital modulation is sensitive to the polytropic exponent Γ . This strongly implies that the cooling efficiency in the accretion disc plays an important role in the X-ray activity in Be/X-ray binaries.

3.3.3 Magnetospheric radius

Changes in the mass flux on the magnetosphere of the neutron star determine whether the system is in the direct accretion regime or in the propeller regime. While the matter falls directly on to the neutron star in the direct accretion regime, no material accretes on to the neutron star in the propeller regime by the centrifugal inhibition. If the magnetospheric radius R_M is smaller than the corotation radius R_Ω , the system is in the direct accretion regime, otherwise, in the propeller regime.

Assuming the neutron star magnetic field as the dipole-like field, the magnetospheric radius R_M , obtained by equating the magnetic field pressure of the neutron star to the ram pressure of the accreting matter from the accretion disc, is written by

$$R_M = 5.1 \times 10^8 k \left(\frac{\dot{M}}{10^{16} \text{ erg s}^{-1}} \right)^{-2/7} \left(\frac{M_X}{M_\odot} \right)^{-1/7} \times \left(\frac{\mu}{10^{30} \text{ G cm}} \right)^{4/7} \text{ cm}, \quad (6)$$

(Pringle & Rees 1972; Lamb, Pethick & Pines 1973; see also Frank et al. 2002), where μ is the magnetic moment. Here, k is a constant model parameter of order unity, depending on the physics and geometry of accretion. For spherical accretion, $k \simeq 0.91$. The original model calculations by Ghosh & Lamb (1979) for disc accretion on to the aligned rotating magnetized neutron star obtained $k \simeq 0.47$, whereas calculations by Ostriker & Shu (1995), which included an induced wind not considered by Ghosh & Lamb (1979), resulted in the value of $k \simeq 0.923$ for disc accretion.

Fig. 14(b) shows the evolution of the magnetospheric radius R_M normalized by the corotation radius R_Ω , where $k = 0.47$ was adopted. In the figure, the thick and thin lines are for models 1 and 2, respectively. Recall that these models have the same parameters except for the radius of the inner simulation boundary r_{in} ; $r_{\text{in}} = 3 \times 10^{-3}$ in model 1, while $r_{\text{in}} = 5 \times 10^{-3}$ in model 2. It should be noted that the magnetospheric radii in both models evolve in a very similar way, despite the different inner radii. Our result on the magnetospheric radius is robust in this sense.

We also note from Fig. 14(b) that the ratio of the magnetospheric radius to the corotation radius, R_M/R_Ω , varies between $\sim k$ and $\lesssim 2k$. Consequently, if $k \sim 0.5$, the magnetospheric radius is almost always larger than the corotation radius and the accretion on to the neutron star is inhibited, which is consistent with the observed X-ray luminosity of 4U 0115+63 in quiescence (Bildsten et al. 1997; Negueruela et al. 2001; Campana et al. 2001). On the other hand, if $k \sim 1$, the magnetospheric radius is almost always smaller than the corotation radius and the neutron star

stays in the direct accretion regime. Then, the system would show a persistent X-ray emission at a level of $\sim 10^{35} \text{ erg s}^{-1}$, which is much higher than the observed X-ray luminosity of 4U 0115+63 in quiescence. Thus, our simulations prefer $k \sim 0.5$.

4 SUMMARY AND DISCUSSION

For the first time, we have performed the numerical simulations of the accretion on to the neutron star in Be/X-ray binaries, taking into account the phase-dependent mass transfer from the Be disc. We have adopted the mass-transfer rate from a high-resolution simulation by Okazaki et al. (2002) for a coplanar system with a short period ($P_{\text{orb}} = 24.3 \text{ d}$) and moderate eccentricity ($e = 0.34$), which targeted 4U 0115+63, one of the best studied Be/X-ray binaries. We have found that a nearly Keplerian, non-steady accretion disc is formed around the neutron star regardless of the parameters adopted. The formation of the accretion disc involves a two-stage process, which consists of the initial developing stage and the later developed stage. The disc structure shows a strong dependence on the orbital phase, because both of the tidal potential and the mass-transfer rate change periodically. The disc is also significantly eccentric, because the gas particles from the Be disc originally have elliptical orbits.

In 4U 0115+63, Type I X-ray outbursts have occurred only as a short series after occasional Type II X-ray outbursts (Negueruela et al. 2001). Except for such occasions, the system is in the quiescent state ($10^{33} - 10^{35} \text{ erg s}^{-1}$) (Campana et al. 2001). The peak X-ray luminosity estimated from our simulations corresponds to the transition regime between the direct accretion regime and the propeller regime and is consistent with the observed X-ray behaviour. Note, however, that the discussion based on the X-ray luminosity estimated from the simulations only gives the necessary condition for the quiescent state.

In order to see whether our model satisfies a more stringent condition, we also have estimated the magnetospheric radius by using a general formula with the mass-accretion rate from our simulations and compared with the corotation radius for 4U 0115+63. The result was that our model with $\Gamma \leq 1.2$ is consistent with the observed X-ray behaviour if $k \sim 0.5$, where $0.5 \lesssim k \lesssim 1$ is a parameter which depends on the geometry and physics of accretion (see equation (6)). Other models with $\Gamma = 5/3$ and $k \geq 0.5$ or with $\Gamma \leq 1.2$ and $k \sim 1$ were ruled out as the model for the quiescent state, because in these models the system enters the direct accretion regime after every periastron passage. We have to admit, however, that the radius of our inner simulation boundary is about 60-100 times as large as the corotation radius of the neutron star in 4U 0115+63. To make the constraint on the system parameters more reliable, we need numerical simulations with a much smaller inner boundary.

It is important to note that our model is not only consistent with the quiescent state of 4U 0115+63. It can also give a natural explanation for a short series of Type I X-ray outbursts after occasional Type II X-ray outbursts. The mass-transfer rate from the Be disc in the X-ray outbursts is likely much higher than in the quiescent state. Suppose that the mass-transfer rate from the Be disc in 4U 0115+63

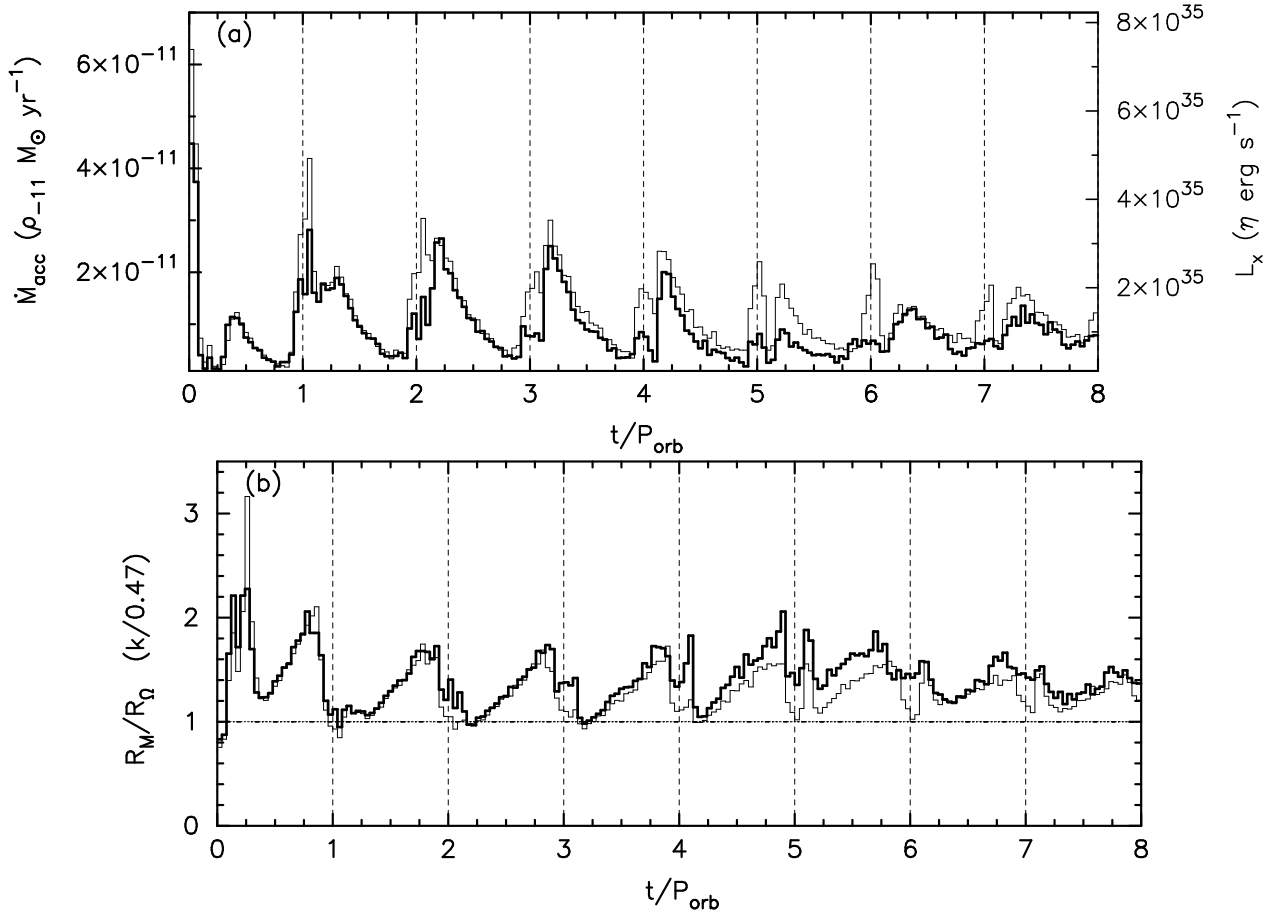


Figure 14. Evolution of (a) the mass accretion rate \dot{M}_{acc} and (b) the ratio of the magnetospheric radius to the corotation radius R_M/R_{Ω} . In each panel, the thick and thin lines are for models 1 and 2, respectively. In Panel (a), the mass-accretion rate is measured in units of $\rho_{-11} M_{\odot} \text{ yr}^{-1}$. The right axis is for the X-ray luminosity corresponding to the mass-accretion rate with $\eta = 1$. In Panel (b), the horizontal dotted line denotes the critical line of $R_M = R_{\Omega}$.

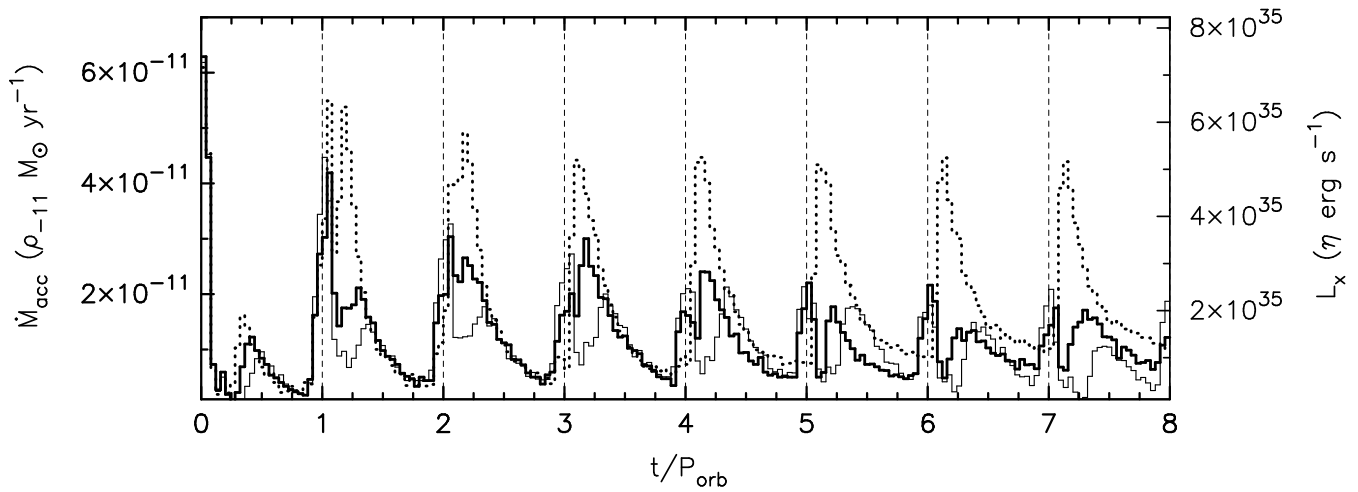


Figure 15. Evolution of the mass-accretion rate \dot{M}_{acc} for models 2-4 with different polytropic exponents. The thick and thin solid lines and the thick dotted line denote the mass-accretion rates for models 2, 3 and 4, respectively. The mass-accretion rate is measured in units of $\rho_{-11} M_{\odot} \text{ yr}^{-1}$. The right axis is for the X-ray luminosity corresponding to the mass-accretion rate with $\eta = 1$.

is temporarily increased by an order of magnitude. Then, the estimated X-ray luminosity in our model increases by an order of magnitude to a level of several $\times 10^{36}$ erg s $^{-1}$, a typical X-ray luminosity of Type I X-ray outbursts. At the same time, the magnetospheric radius R_M decreases by a factor of about two, for which R_M is almost always smaller than the corotation radius, R_Ω , even if $k \sim 0.5$ (see Fig. 14(b)). This means that the system is in the direct accretion regime. Thus, our model explains the Type I X-ray outbursts in 4U 0115+63 as a temporal phenomena with an enhanced mass-transfer from the Be disc.

Be/X-ray binaries are distributed over a wide range of orbital periods ($16 \text{ d} \lesssim P_{\text{orb}} \lesssim 243 \text{ d}$) and eccentricities ($e \lesssim 0.9$). It is interesting to consider here the effects of orbital parameters. In this paper, we have seen that the main ingredients which determines the X-ray behaviour of a system are the viscous time-scale relative to the orbital period and the mass-transfer rate from the Be disc. Since the former is insensitive to the orbital period itself (see equation (4)), the latter is most important if the viscosity parameter and the equation of state are similar in accretion discs of Be/X-ray binaries.

In systems with $\alpha_{\text{SS}} \lesssim 0.1$, the viscous time-scale in an outer part of the accretion disc is much longer than the orbital period unless the cooling is ineffective and the gas obeys an adiabatic equation of state. In these systems, persistent accretion discs are expected to form. Then, the mass-transfer rate from the Be disc determines whether the system shows Type I X-ray outbursts. For example, for a system with a moderate orbital eccentricity of $e = 0.34$ and a typical density of Be disc, the peak mass-transfer rate is $\sim 2 \times 10^{-10} M_\odot \text{ yr}^{-1}$, for which the system stays in quiescence. It is obvious, however, that the situation should be different in systems with much higher rate of mass-transfer. A high mass-transfer rate is expected to result from a high orbital eccentricity and/or an intrinsically dense Be disc. Therefore, it is no strange that many systems which have regularly shown Type I X-ray outbursts have orbital eccentricities higher than that of 4U 0115+63 studied in this paper. In a subsequent paper, we will perform numerical simulations of accretion in systems with high orbital eccentricities.

Above we have assumed that the viscous time-scale is much longer than the orbital period in all Be/X-ray binaries. However, it is possible that an accretion disc has a relatively short viscous time-scale by some reason. One possibility is that the disc has a low cooling efficiency and becomes hot, particularly in an inner region. Our model 4 with $\Gamma = 5/3$ gives an extreme example of such discs. As shown in Fig. 15, in a system with a short viscous time-scale, the mass-accretion rate has a high and sharp peak shortly after every periastron passage. The resemblance between the accretion rate profile in model 4 and the X-ray light curves of regular Type I X-ray outbursts from systems such as EXO 2030+375 (Wilson et al. 2002) implies that these are systems with relatively short viscous time-scales.

Be/X-ray binaries are an ideal group of objects for studying the physics of accretion under the circumstances which have been studied little. Unlike close binaries, many Be/X-ray binaries have eccentric orbits. They can also be highly inclined systems. Such systems provide us a valuable opportunity to study the effects of the periodically-changing

tidal potential and mass-transfer rate and the inclination angle on the structure and evolution of the accretion flow. Another important characteristic of Be/X-ray binaries is that they are systems with double circumstellar discs (the Be disc and the accretion disc). The interaction in such systems is threefold: the interactions between the neutron star and the Be disc, the Be star and the accretion disc and the Be disc and the accretion disc (mainly via the mass transfer). Much more work is desirable both theoretically and observationally in order to understand this interesting and important group of objects.

ACKNOWLEDGEMENTS

KH acknowledges James R. Murray for useful comments during the short stay at the Swinburne University of Technology, Australia. The simulations reported here were performed using the facility at the Hokkaido University Information Initiative Center, Japan. This work was supported in part by Grant-in-Aid for Scientific Reserch (13640244) of Japan Society for the Promotion of Science.

REFERENCES

- Artymowicz P & Lubow S.H., 1994, ApJ, 421, 651
- Bate M.R., Bonnell I.A., Price N.M., 1995, MNRAS, 285, 33
- Benz W., 1990, in Buchler J. R., ed., The Numerical Modelling of Nonlinear Stellar Pulsations. Kluwer, Dordrecht, p.269
- Benz W., Bowers R.L., Cameron A.G.W., Press W.H., 1990, ApJ, 348, 647
- Bildsten, L., Chakrabarty, D., Chiu, J., et al. 1997, ApJS, 113, 367
- Campana S., Gastaldello F., Stella L., Israel G.L., Colpi M., Pizzolato F., Orlandini M., Dal Fiume D., 2001, ApJ, 561, 924
- Clark J.S., Lyuty V.M., Zaitseva G.V., Larionov V.M., Larionova L.V., Finger M., Tarasov A.E., Roche P., Coe M.J., 1999, MNRAS, 302, 167
- Finger M.H., Wilson R.B., Harmon B.A., 1996, ApJ, 459, 288
- Finger M.H., Bildsten L., Chakrabarty D., Prince T.A., Scott D.M., Wilson C.A., Wilson R.B & Zhang S.N., 1999, ApJ, 517, 449
- Frank J., King A.R., Raine D.J., 2002, Accretion power in Astrophysics, 3rd edn. Cambridge Univ. Press, Cambridge
- Ghosh P & Lamb F.K., 1979, ApJ, 234, 296
- Lamb F.K., Pethick C.J & Pines D., 1973, ApJ, 184, 271
- Negueruela I., Okazaki A.T., Fabregat J., Coe M.J., Munari U & Tomov., 2001, A&A, 369, 108
- Negueruela I & Okazaki A.T., 2001, A&A, 369, 108
- Okazaki A.T & Negueruela I., 2001, A&A, 377, 161
- Okazaki A.T., Bate M.R., Ogilvie G.I & Pringle J.E., 2002, MNRAS, 337, 967
- Ostriker E.C., Shu F.H., 1995, 447, 813
- Pringle J.E & Rees M.J., 1972, A&A, 21, 1
- Stella L., White N.E., Rosner R., 1986, ApJ, 208, 669
- Warner B., 1995, Cataclysmic Variable Stars. Cambridge Univ. Press, Cambridge

- Wilson C.A & Finger M.H., Coe M.J., Laycock S., Fabregat J., 2002, *ApJ*, 570, 287
Wilson C.A & Finger M.H., Coe M.J., Negueruela I., 2003, *ApJ*, 584, 996
Ziolkowski J., 2002, *Mem. Soc. Astron. Ital*, 73, 1038